CEPHEID VARIABLES IN M33 AND THE EXTRAGALACTIC DISTANCE SCALE

A Senior Scholars Thesis

by

ANDREW KENNETH BRADSHAW

Submitted to the Office of Undergraduate Research at
Texas A&M University
in partial fulfillment of the requirements for the designation as

UNDERGRADUATE RESEARCH SCHOLAR

April 2009

Major: Physics

CEPHEID VARIABLES IN M33 AND
THE EXTRAGALACTIC DISTANCE SCALE

A Senior Scholars Thesis

by

ANDREW KENNETH BRADSHAW

Submitted to the Office of Undergraduate Research at
Texas A&M University
in partial fulfillment of the requirements for the designation as

UNDERGRADUATE RESEARCH SCHOLAR

Approved by:

Research Advisor: Lucas Macri
Associate Dean for Undergraduate Research: Robert C. Webb

April 2009

Major: Physics

ABSTRACT

Cepheid Variables in M33 and the Extragalatic
Distance Scale. (April 2009)

Andrew Kenneth Bradshaw
Department of Physics
Texas A&M University

Research Advisor: Dr. Lucas Macri
Department of Physics

Cepheid variables constitute the first rung of the extragalactic distance scale. As such, they can be used to determine distances to nearby galaxies and calibrate secondary distance indicators, such as type Ia supernovae. A detailed study of Cepheids in nearby galaxies is required in order to properly characterize their properties and variations as a function of secondary parameters (such as metallicity).

One such nearby galaxy, M33, was observed by the DIRECT project as part of a long-term program to improve the extragalactic distance ladder. We present the detection of Cepheids and other variables in one field of M33 observed by the project.

The analysis consisted of point-spread function photometry of hundreds of individual images which were referenced to a master frame, followed by the application of statistical techniques to determine the variability of the stars that were detected. Since this region of the galaxy was imaged over three consecutive observing seasons, we were able to search for long-period variables in addition to Cepheids.

Our results include a color-magnitude diagram of the field, light curves of Cepheids

and some of the interesting long-period variables and Period-Luminosity relations. We use the latter to estimate the distance to M33.

TABLE OF CONTENTS

LIST OF FIGURES

FIGURE   Page

CHAPTER I

INTRODUCTION

With the large size of the Universe comes a great diversity in the types of objects that populate it. One of the most important and useful astronomical objects are variable stars; stellar objects which, over time, change their brightness. This change in brightness can then be measured and quantified. Historically this was done using photographic plates or even with eye-observation; now measurements are made with modern imaging technology, such as CCDs (Charge-Coupled Devices). Once the properties of the object (i.e., period of oscillation, rate of change, etc.) are known, they can sometimes be related to other more fundamental quantities.

The name 'variable star' can refer to a wide variety of objects, including supernovae, eclipsing binary stars, or even transiting planets. However, this thesis will be focused on a specific type of variable star, called a Cepheid variable, which has a characteristic light curve and a well-defined periodicity ranging from a few days to a few months. Other variable objects found will also be presented and discussed.

The goal of this research project is to detect and classify Cepheid variable stars in the nearby spiral galaxy M33, also called the Triangulum Galaxy, shown in Figure 1. Due to the correlation between their period of variability and their luminosity, measuring the brightness of Cepheids over time presents an opportunity to derive accurate distances to objects outside of our Milky Way. Using these Cepheid-based distances and related measurements, we can infer distances to more distant galaxies

This thesis follows the style and format of The Astrophysical Journal.

and ultimately build a cosmic distance scale with which the overall properties of our Universe can be investigated.

History of variable stars

Variable stars have only recently come under the scrutiny of scientists, though they were perhaps noticed long ago. This is because, excluding supernovae and novae (which are non-periodic objects), variable stars are often too nearly constant for the eye to discriminate. Thus the first periodic variable star known to Western civilization, o Ceti, was only discovered in the early 17th century shortly after the invention of the telescope. A flurry of variable star discoveries followed, but the situation did not change much until the invention and use of photographic plates.

However, around 1782 a deaf British amateur astronomer by the name of John Goodricke surprised the scientific world with the confirmation of two new variable stars, β Lyrae and β Persei. Shortly thereafter he found a new peculiar type of variable star, δ Cephei, whose light curve exhibited a shape different than those discovered before. This class of stars, later named Cepheids after the prototypical δ Cephei, were in the early 1900's found to be intrinsically pulsating rather than the familiar binary system eclipses.

Cepheids finally became a useful phenomena, rather than an oddity, when in 1912 Henrietta Leavitt discovered a correlation between the apparent brightness and period of Cepheids in the Small Magellanic Cloud (Leavitt & Pickering 1912). A modern version of this relation is shown in Figure 2. This relation is now commonly referred to as the Cepheid Period-Luminosity (P-L) relation and it allows one to derive the
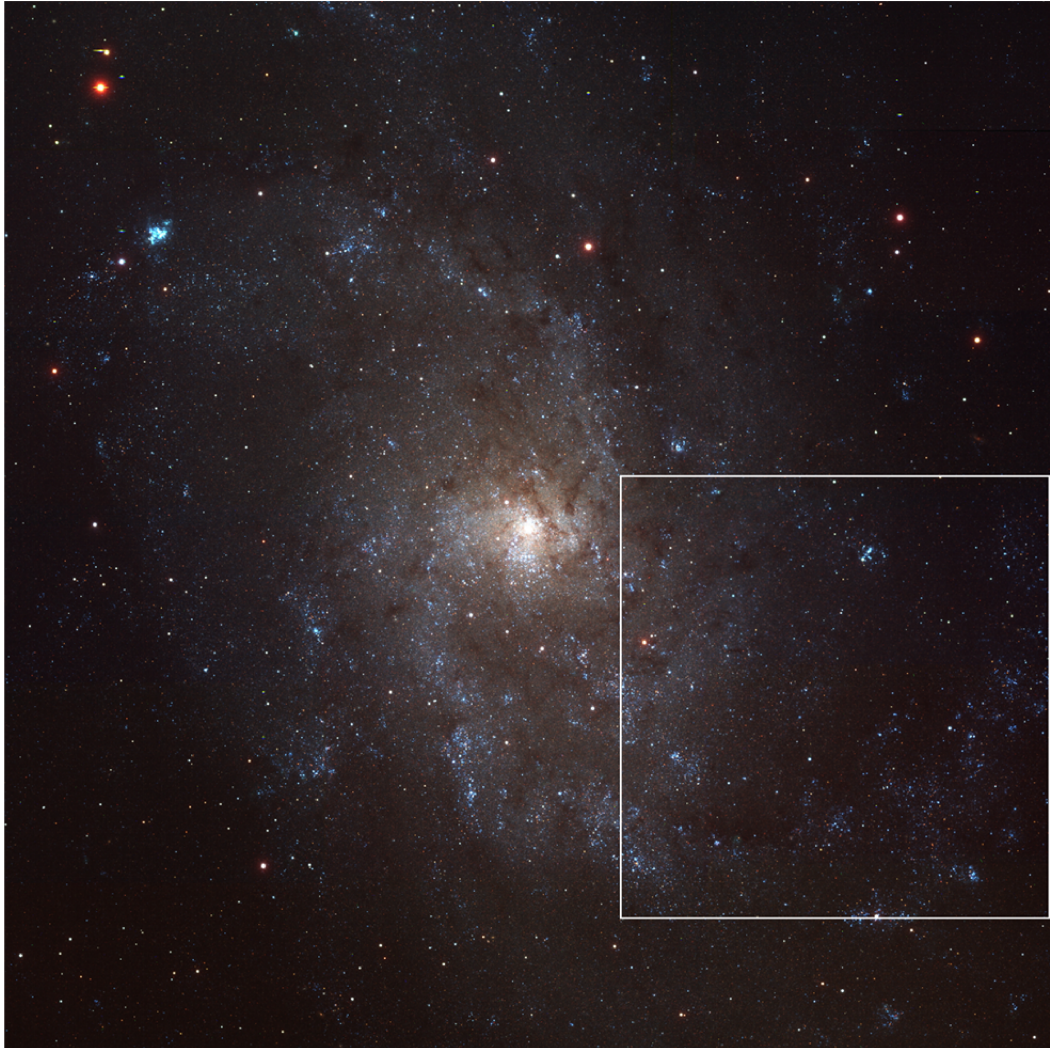
FIG. 1.— A mosaic of M33 indicating the location of our field (white rectangle). Its size is 11' x 11'.

luminosity of a Cepheid once its period is known. By comparing the stellar flux (a distance-dependent quantity) with its derived luminosity, the distance to the object can be estimated.

Applications of Cepheid variables

It was in 1926 that Edwin Hubble presented his discovery of Cepheid variables in Local Group galaxies which were previously believed to be 'nebulae' within our own Milky Way. Then, using the P-L relation set forward by Leavitt, he showed that these objects must be far outside of our own Milky Way galaxy. Later, he attempted to calibrate a "secondary distance indicator" (the luminosity of the brightest star in a galaxy) to determine the distances of more distant galaxies. He coupled these distances to velocities that had been measured through spectral Doppler shifts by Slipher, and found a striking relation: the further away a galaxy is, the larger the Doppler shift of the galaxy was (Hubble 1929). Using Einstein's equations of General Relativity, this lead directly to the confirmation of the Big Bang theory presented by Friedmann in 1922. All Cepheid distance measurements made today follow this simple process first set out by Dr. Hubble.

Interestingly, the usefulness of Cepheid variables can be purely left to an empirical basis. An understanding of the physical mechanism behind the variability, though an interesting problem, was not necessary for their initial application. However, eventually the problem was solved and simultaneously provided insight into the evolution of stars as a whole. Originally these strange periodic variable stars were thought to be binary star eclipsing events, perhaps because stars were considered to be such perfect and constant sources of light. This binary hypothesis was later abandoned of course,
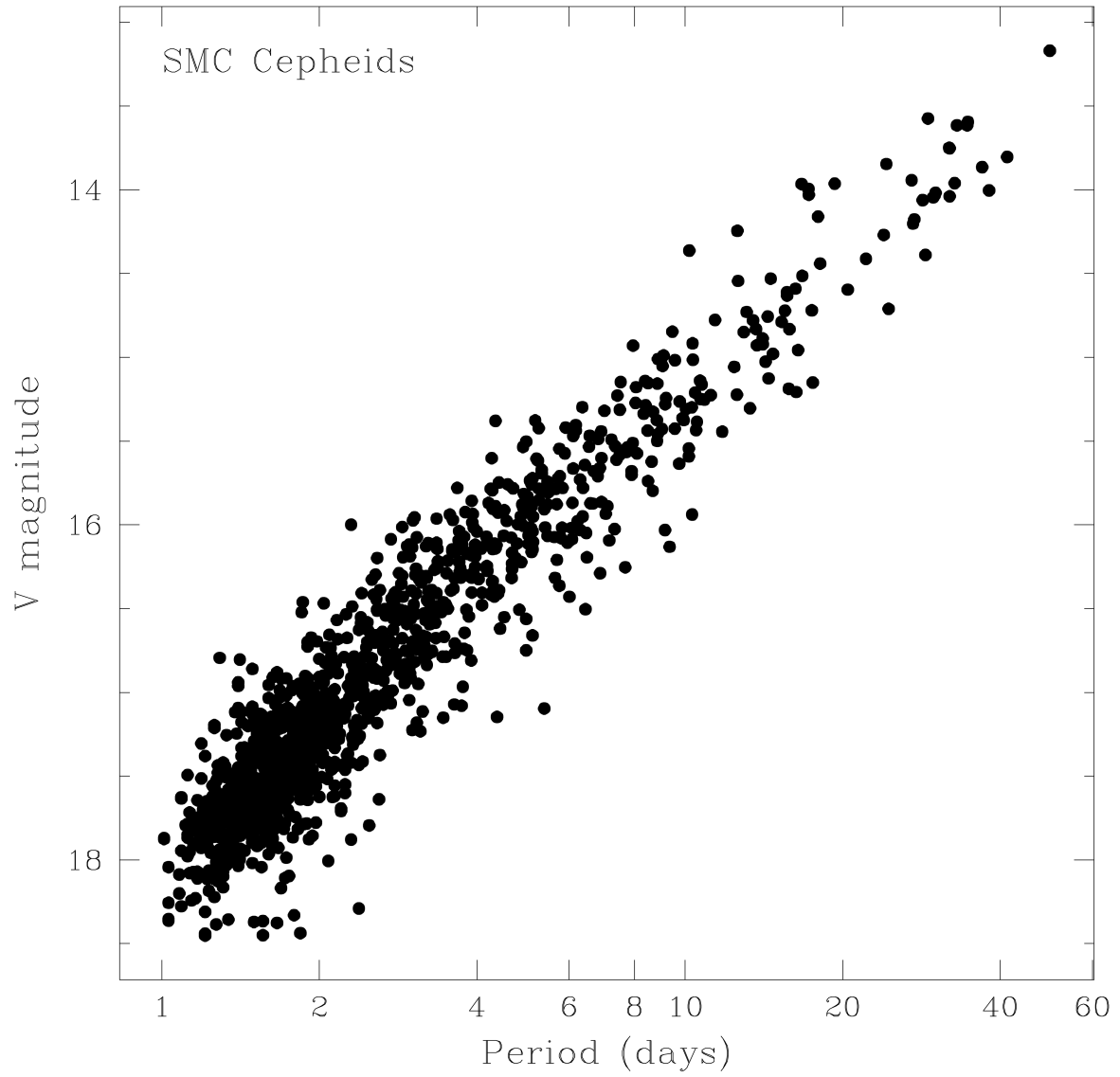
FIG. 2.— A period-luminosity relation for Cepheids in the small magellanic cloud, from Udalski et al. (1999).

along with similar hypotheses requiring the rotation of sunspots across the surface of the star. The true mechanism of their variability was not known until Eddington put forward several models in the 1920's. After failing to describe their long-lived pulsation using simple Newtonian dynamics and pressure laws, Eddington modeled the Cepheid as a star with layers of ionizable gas. The so called κ-mechanism (Eddington 1930) describes shells within the star that are partially ionized. When gravitationally compressed, the regions tend to use some of the work from compression to ionize, instead of heat up, the layer. This disrupts the star's equilibrium and pushes the layers outward until ionization (and thus opacity) decreases, which leads to gravitational collapse back to the beginning of the cycle. This process is shown graphically in Figure 3. The various points along the curve indicate major changes in stellar processes, as follows: A: Star cannot halt gravitational collapse, begins contracting. B: Star continues collapsing and more heat is generated, ionization increases and thus opacity increases. C: Opaque layers are pushed outward due to radiation pressure. D: Outward acceleration slows, and gravitational collapse beings again.

But how does a star become a Cepheid variable in the first place? Figure 4 displays a so-called "Hertzsprung-Rusell" diagram which plots the temperature and luminosity of stars. The track plotted in this figure represents the different positions over time for a star of 7 solar masses. After its pre-main sequence evolution (points a-c) the star spends the majority of its life at point (d) where it fuses hydrogen to helium in its core. Once this reservoir of fuel is exhausted, it starts a rather convoluted post-main sequence evolution during which it crosses a region known as the "instability strip" which is represented by two dashed lines in that figure. It is only within this narrow range of temperature that stable pulsations (as described above) can take place. The Cepheid phase of the star takes place between points (h) and (j) in the diagram.
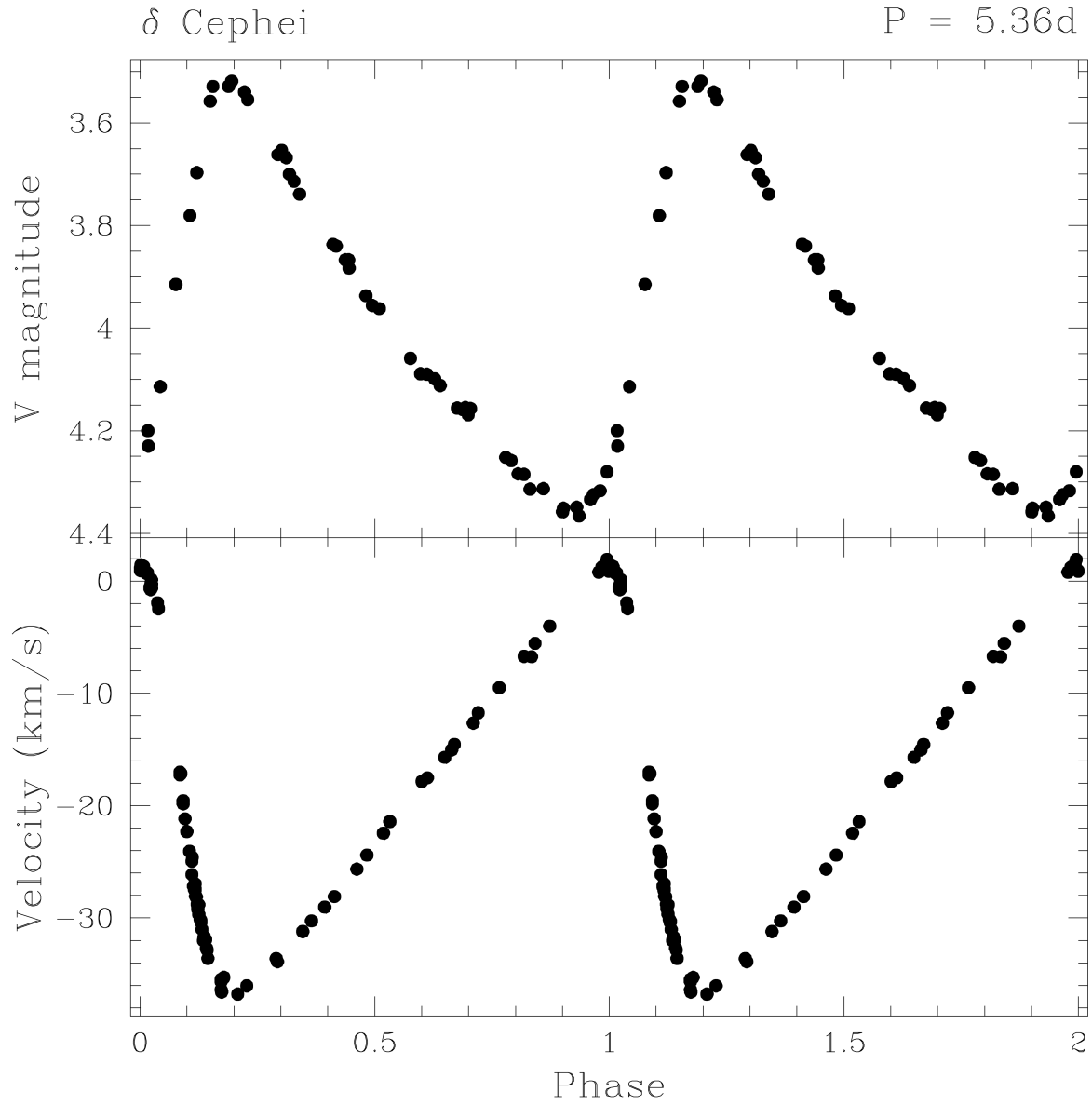
FIG. 3.— Light (top) and radial velocity (center) curves for δ Cephei. The bottom pannel shows a schematic representation of the oscillation.
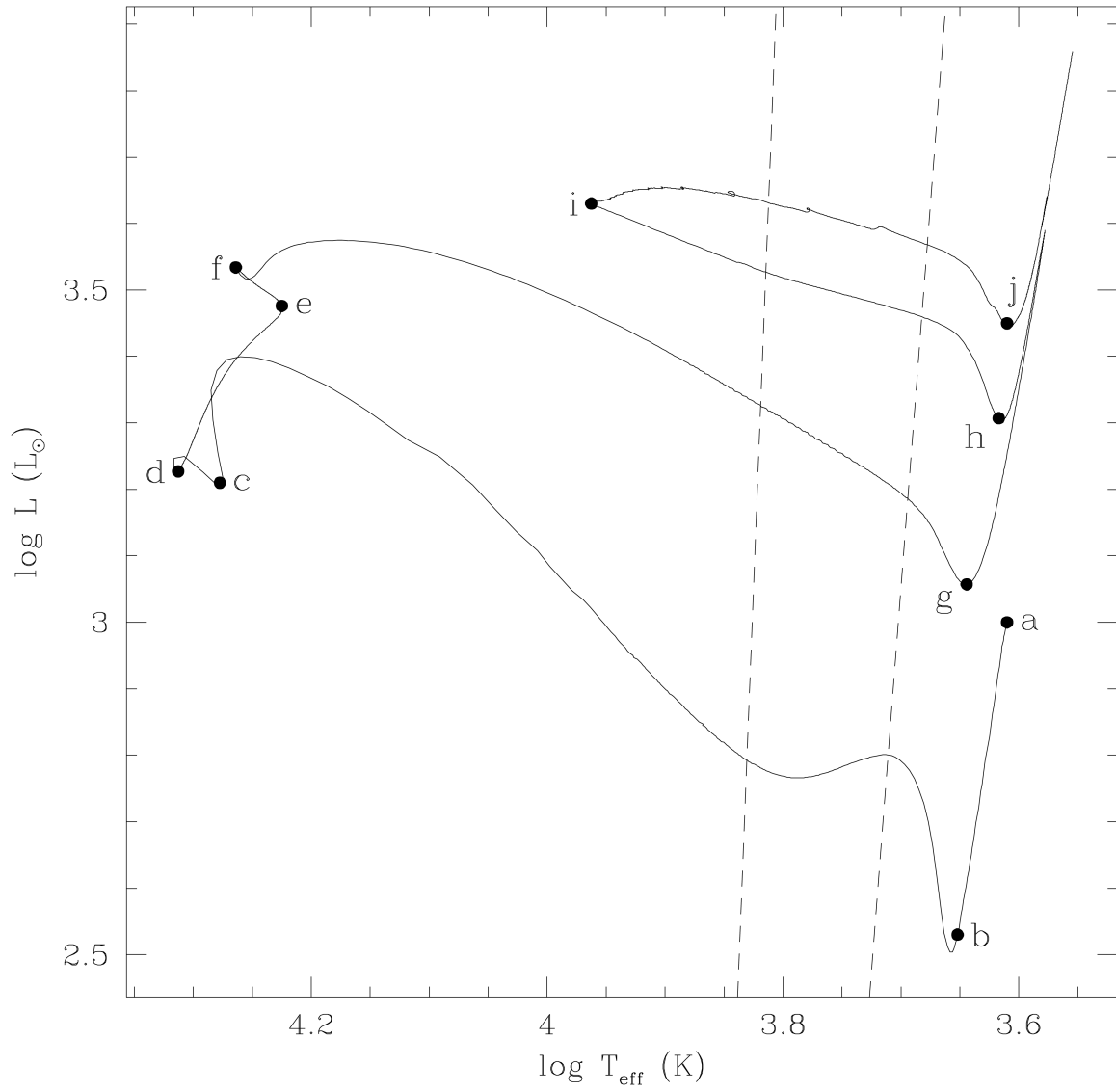
FIG. 4.— Evolutionary track of a 7-solar-mass star based on the models of Siess et al. (2000) and Alibert et al. (1999).

The Cepheid phase is therefore a transient phenomena experienced only by stars with masses between 5 and 12 times that of the Sun. Because of this, relatively few stars are exhibiting this behavior at any given time. Out of a hundred billion stars in our Galaxy it is estimated that there are only a few million pulsating stars (and even fewer Cepheid variables), indicating that variability is around a .001 percent effect in any given sample. These odds are slightly improved when considering that most Cepheids are supergiant stars with high luminosities, but the effect still remains rare. This is the reasoning behind comprehensive star surveys, such as the one in this thesis, which must be mounted to discover these special stars within a particular galaxy.

Project overview

The observations used in this thesis were obtained as part of the DIRECT project, an initiative to calibrate the Cepheid Period-Luminosity relation with greater accuracy by discovering large samples of these stars in the nearby galaxies M31 and M33. The observations were made using the F.L. Whipple Observatory's 1.2 meter telescope between September 1996 and December 2000. Three different broadband filters were used during observation: V, I, and B. Within each band the project obtained 265, 78, and 35 images, respectively, resulting in several gigabytes worth of data. The raw data was corrected for several instrumental characteristics, including the removal of electronic noise (bias correction) and fluctuations in the relative sensitivity of each pixel in the array (flat-fielding).

After the data was properly reduced, each image was processed to detect all stars within it and to determine its particular orientation relative to a user-specified reference frame. We carried out these procedures using the DAOPHOT/ALLFRAME

suite of programs developed by Peter Stetson. Once the photometry had been obtained, we performed additional photometric corrections and searched for variables in the data. Lastly, an automated procedure classified some of these variables as Cepheids, which were eventually used to form multi-band Period-Luminosity relations and estimate the distance to M33.

CHAPTER II

THEORY

This chapter is meant to flesh out some of the mathematical details behind stellar pulsation in general. Though such details have long been known and understood, their derivation can still provides useful insight. In this chapter we look into the actual mechanisms that allow stars to be such consistent and long-lived objects, while at the same time modeling their instability.

Using tools such as thermodynamics and Newton's laws we are able to make two separate approximations, both leading to a rough sketch of stellar pulsation. The first model assumes that the pulsation is due to acoustic waves propagating through the star and then infers the pulsational period. The second method, a little more complex, does not make such assumptions. Rather it is a perturbation of the basic hydrodynamic model of stars. Both methods arrive at similar (and roughly correct) pulsational periods for a given mass and radius (or density). Because the pulsational period is the physical quantity we observe, knowing its mechanism can provide some insight into the physics behind stellar pulsation.

Hydrostatic equilibrium

Before we begin to pulsate our star it is important that we establish the basics. All stars are basically balls of gas which are in a constant balancing act: gravity pulls the outer layers of gas inward and pressure pushes the layers outward. A force diagram of this situation is shown in Figure 5.
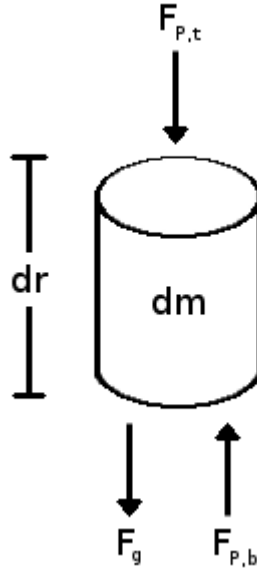
FIG. 5.— A force diagram for a mass element dm with radius dr.

Using Newton's Second Law, we start with Equation 2.1:

$$dm\frac{d^2r}{dt^2} = \Sigma F = F_g + F_{P,t} + F_{P,b}. \tag{2.1}$$

We then make the substitution $F_{P,t} = -(F_{P,b} + dF_p)$, where dF_p accounts for the pressure difference between r and $r + dr$, so that

$$dm\frac{d^2r}{dt^2} = F_g - F_{P,b} - dF_p + F_{P,b} = F_g - dF_p. \tag{2.2}$$

But we also know that $\frac{dF_p}{A} = dP$ and that $F_g = -G\frac{M_r dm}{r^2}$, where $M_r = \int_0^r 4\pi r^2 dm dr$. Also we can substitute for the mass dm the density equation $dm = Adr\rho$. Thus we end up with an equation for radial motion, Equation 2.4:

$$Adr\rho\frac{d^2r}{dt^2} = -G\frac{M_r \rho Adr}{r^2} - AdP \tag{2.3}$$

or, after dividing by volume,

$$\rho\frac{d^2r}{dt^2} = -G\frac{M_r\rho}{r^2} - \frac{dP}{dr}. \tag{2.4}$$

However, we assume the star to be in equilibrium so that $a = 0$, or, $\Sigma F = 0$:

$$\frac{dP}{dr} = -G\frac{M_r\rho}{r^2} = -\rho g \tag{2.5}$$

where $g \equiv G\frac{M_r}{r^2}$. Equation 2.5 is the equation for hydrostatic equilibrium. This equation shows that it is actually the pressure gradient, rather than simply the pressure, which prevents the star from collapsing. Finally, assuming the (unrealistic) case of constant density throughout the star so that $M_r = \frac{4}{3}\pi r^3\rho$, Equation 2.5 becomes

$$\frac{dP}{dr} = -G\frac{M_r\rho}{r^2} = -\frac{4}{3}\pi G\rho^2 r \tag{2.6}$$

which we will use later.

First approximation: acoustic oscillations

Now we can implement one of the simplest models of stellar pulsation. This model assumes that the pulsations are purely radial and are the result of sound waves (pressure/density waves) resonating within a star. To begin with this assumption we must first calculate the speed of sound within the star then find the time it takes to cross the entire diameter (which becomes the period of pulsation). But how do we calculate the speed of sound in a star? Consult the First Law of Thermodynamics:

$$dU = \delta Q - \delta W \tag{2.7}$$

We then approximate the oscillations as adiabatic (i.e. no heat transfer), and therefore we set $\delta Q = 0$. Also we know that the differential work is equal to the differential

volume change times the pressure, $\delta W = PdV$. Thus

$$dU = -PdV. \tag{2.8}$$

We now use the ideal gas equation $PV = nkT$, in differential form

$$VdP + PdV = nkdT \tag{2.9}$$

and heat capacity relation

$$dU = C_v dT \quad \Rightarrow \quad dT = \frac{dU}{C_v} = -\frac{PdV}{C_v}. \tag{2.10}$$

We know that $C_p = C_v + nk$ and that $\gamma \equiv \frac{C_p}{C_v}$, so that $\gamma = 1 + \frac{nk}{C_v}$, which we use in the equation for adiabatic gases, Equation 2.12:

$$Vdp = 1 - \gamma - Pdv \tag{2.11}$$

$$\gamma \frac{dV}{V} = -\frac{dP}{P} \tag{2.12}$$

The speed of sound in a material is related to its compressibility (or bulk modulus) $\kappa \equiv -V\frac{dP}{dV}$ and its density ρ such that

$$v_{sound} = \sqrt{\frac{\kappa}{\rho}} = \sqrt{\frac{\gamma P}{\rho}} \tag{2.13}$$

where Equation 2.12 has been used. But according to Equation 2.13 v_{sound} depends on P, which depends on the radius r, according to the following equation:

$$\frac{dP}{dr} = -\frac{4\pi}{3}G\rho^2 r \quad \underrightarrow{integrate} \quad \int_R^r dP = -\frac{4\pi}{3}G\rho^2 \int_R^r r'dr'. \tag{2.14}$$

Assuming that $P = 0$ at $r = R$, then we are led to the following equation for pressure

P as a function of radius r:

$$P(r) = \frac{2\pi}{3}G\rho^2(R^2 - r^2) \tag{2.15}$$

and to the equation for v_{sound} as a function of r:

$$v_{sound} = \sqrt{\frac{2\pi}{3}\gamma G\rho(R^2 - r^2)}. \tag{2.16}$$

Finally, we can use this velocity to determine the time it takes for an adiabatic pressure wave to cross the diameter of the star:

$$\Pi \approx 2\int_0^R \frac{dr}{v_{sound}}. \tag{2.17}$$

Using the equation above and inserting Equation 2.16 we arrive at:

$$\Pi \approx 2\int_0^R \frac{dr}{\sqrt{\frac{2\pi}{3}\gamma G\rho(R^2 - r^2)}} \tag{2.18}$$

$$= \frac{2}{\sqrt{\frac{2}{3}\gamma\pi G\rho R^2}}\int_0^R \frac{dr}{\sqrt{1 - (\frac{r}{R})^2}} \tag{2.19}$$

$$= \frac{2}{\sqrt{\frac{2}{3}\gamma\pi G\rho R^2}}\int_0^R \frac{R\cos\theta d\theta}{sqrt1 - sin^2\theta} \tag{2.20}$$

$$= \frac{2}{\sqrt{\frac{2}{3}\gamma\pi G\rho R^2}}\int_0^R \frac{R\cos\theta d\theta}{\cos\theta} \tag{2.21}$$

$$= \frac{2}{\sqrt{\frac{2}{3}\gamma\pi G\rho}}\ [\sin^{-1}(\frac{r}{R})|_0^R \tag{2.22}$$

$$= \sqrt{\frac{3\pi}{2\gamma G\rho}} \tag{2.23}$$

where in the above equations we used the substitution $r = R\sin\theta$ and $dr = R\cos\theta d\theta$.

The final line, Equation 2.23, illustrates the period-density relation. It shows that as the density of a star increases so does its period. Qualitatively this is confirmed by

observation: giant and supergiant stars, having smaller densities, have longer periods than the much more dense white dwarf stars. Quantitatively we can use the example of a star with typical Cepheid properties of $M = 5M_\odot$ and $R = 50R_\odot$. Plugging these numbers into equation 2.23 yields a period of ≈ 10 days, which is reasonable considering the typical properties used. We now move on to a slightly more complex derivation of stellar pulsation.

Second approximation: perturbations

The previous model had a major problem with it in assuming that the radius is fixed and that the star ultimately remains in equilibrium during the pulsations. Observations have shown that this is clearly not the case, with a typical Cepheid star changing in radius as much as a few percent. In this model we assume then that the radius changes are small and then perform a perturbation of the radius such that:

$$r_0 \quad \rightarrow \quad r(t) \quad = \quad r_0[1 + \Delta(t)] \tag{2.24}$$

$$dr \quad = \quad dr_0[1 + \Delta(t)]. \tag{2.25}$$

Similarly we can perturb the density, assuming that there is no mass loss out of the (now moving) shell at radius r:

$$\rho 4\pi r^2 dr = \rho_0 4\pi r_0^2 dr_0 \quad \rightarrow \quad \rho = \rho_0[1 + \Delta(t)]^{-3}. \tag{2.26}$$

Again we assume (slightly unrealistically) that the expansion is adiabatic in that there is no energy or heat transfer between the shells. From thermodynamics we get that:

$$\frac{P}{P_0} = (\frac{\rho}{\rho_0})^\gamma \quad \rightarrow \quad P = P_0(\frac{\rho}{\rho_0})^\gamma \tag{2.27}$$

Bringing all of these perturbations together and Taylor expanding them (assuming that Δ is small):

$$\rho = \rho_0(1 - 3\Delta) \tag{2.28}$$

$$P = P_0(1 - 3\gamma\Delta) \tag{2.29}$$

$$r^{-2} = r_0^{-2}(1 - 2\Delta) \tag{2.30}$$

But simply perturbing won't be enough. Because we assume now that the radius is changing, we must also get rid of the requirement that $a = \frac{d^2r}{dt^2} = 0$ and $\Sigma F = 0$. Looking back at Equation 2.4 we can say, after multiplying by dV:

$$\underbrace{\frac{dP}{dr}}_{pressure} = \underbrace{-\frac{GM_r dm}{r^2}\rho}_{gravitational} - \underbrace{\rho\frac{d^2r}{dt^2}}_{inertia} \tag{2.31}$$

The pressure term on the left of Equation 2.31, $\frac{dP}{dr}$ can be re-expressed using the chain rule and another Taylor expansion as follows:

$$\frac{dP}{dr} = \frac{dP}{dr_0}\frac{dr_0}{dr} = \frac{dP_0}{dr_0}(1 - 3\gamma\Delta)(1 - \Delta) \tag{2.32}$$

$$= \frac{dP_0}{dr_0}[1 - \Delta(3\gamma + 1)] \tag{2.33}$$

where second order terms in Δ have been thrown out. But we also know from hydrostatic equilibrium (Equation 2.5) that

$$\frac{dP_0}{dr_0} = -\frac{GM_{r_0}}{r_0^2}\rho_0 \tag{2.34}$$

so that our perturbation of the pressure term of Equation 2.31 becomes

$$\frac{dP}{dr} = -\frac{GM_{r_0}}{r_0^2}[1 - \Delta(3\gamma + 1)]. \tag{2.35}$$

Now insert the perturbation into the gravitational term of Equation 2.31

$$-\frac{GM_r dm}{r^2}\rho = -\frac{GM_{r_0} dm}{r_0^2}\rho_0(1-2\Delta)(1-3\Delta) \tag{2.36}$$

$$= -\frac{GM_{r_0} dm}{r_0^2}\rho_0(1-5\Delta) \tag{2.37}$$

where again second order Δ terms have been thrown out. Finally, apply the perturbation to the inertial term of Equation 2.31:

$$-\rho\frac{d^2 r}{dt^2} = -\rho_0(1-3\Delta)r_0\frac{d^2\Delta}{dt^2}. \tag{2.38}$$

Now put all of these terms from Equations 2.35, 2.37, and 2.38 back into our equation of motion, Equation 2.31, to get:

$$-\frac{GM_{r_0}}{r_0^2}\rho_0[1-\Delta(3\gamma+1)] = -\frac{GM_{r_0}}{r_0^2}\rho_0(1-5\Delta) - \rho_0(1-3\Delta)r_0\frac{d^2\Delta}{dt^2}. \tag{2.39}$$

Solving, we get:

$$-\frac{GM_{r_0}}{r_0^2}\Delta\frac{(3\gamma-4)}{(1-3\Delta)} = r_0^2\frac{d^2\Delta}{dt^2}$$

$$\Rightarrow \frac{GM_{r_0}}{r_0^3}(4-3\gamma)\Delta = \frac{G}{\frac{4\pi}{3}}\rho\Delta(4-3\gamma) = \frac{d^2\Delta}{dt^2}. \tag{2.40}$$

where we made the substitution $\rho = \frac{M}{\frac{4\pi}{3}r^3}$. Cleaning things up a little bit, we arrive at the following differential equation in terms of Δ:

$$\frac{d^2\Delta}{dt^2} + \frac{9G\rho}{4\pi}(\gamma-\frac{4}{3})\Delta = 0. \tag{2.41}$$

This differential equation is analogous to the simple harmonic motion of a spring with a mass attached. The solutions are waves of the form $\Delta(t) = \Delta_0 e^{i\omega t}$, where $\omega^2 = \frac{9G\rho(\gamma-\frac{4}{3})}{4\pi}$. Using the known relation between the period and frequency, $\Pi = \frac{2\pi}{\omega}$,

we are led to the final equation for the period of oscillations:

$$\Pi = \sqrt{\frac{16\pi^3}{9(\gamma - \frac{4}{3})}\frac{1}{G\rho}} \qquad (2.42)$$

or more simply:

$$\Pi \propto (G\rho)^{-\frac{1}{2}}. \qquad (2.43)$$

At first sight this result is very similar to Equation 2.23. However, one important difference lies in the solution of Equation 2.41 where ω has been found to include the term $\gamma - \frac{4}{3}$. Because of this, solutions that are stable exist only for $\gamma > \frac{4}{3}$. Stability in this case means that the star returns to equilibrium after a small perturbation, and in most cases $\gamma = \frac{5}{3}$ which keeps the star stable. However, if γ is less than $\frac{4}{3}$, then the solution of the differential equation becomes a damped exponential of the form $\Delta(t) = \Delta_0 e^{-\kappa t}$. Thus the star actually collapses because gravitational forces overcome the outward pressure. This case of $\gamma \leq \frac{4}{3}$ is extremely interesting, as it actually explains a special type of supernovae, called a core-collapse supernova, which occurs in supergiant stars.

The period luminosity relationship

We can take the derivation of the pulsation period a little further and roughly derive the Period-Luminosity relationship which is much more useful observationally, as we can't actually measure the density of a star! Starting with Equation 2.43:

$$\Pi \propto \rho^{-\frac{1}{2}} \propto M^{-\frac{1}{2}}R^{-\frac{3}{2}} \propto R^{-\frac{3}{2}} \propto L^{-\frac{3}{4}} \qquad (2.44)$$

where we have used the relationship between density and mass/radius and the black-body relationship $L = 4\pi\sigma R^2 T^4 \propto R^2$. But we also know that $M_v = -2.5 \log L_v +$

const. so:

$$M_v = -2.5 \log L_v + C \tag{2.45}$$

$$= -2.5\left(\frac{4}{3}\log \Pi\right) + D \tag{2.46}$$

$$= -\frac{20}{6}\log \Pi + D \approx -3\log \Pi + D \tag{2.47}$$

which is remarkably close to the actual equation for (galactic) Cepheids $M_v = -2.81 \log \Pi - 1.6$.

Physical mechanism

In this section we finally delve into the actual mechanism driving the pulsations. Though we simplistically assumed in the first section that the pulsations are due to sound waves, how would such sound waves be carried? Or, in our second model, what property of the star acts as the 'spring' in our simple model?

But first, why couldn't observations be described by the simple binary-star hypothesis popular in the 19th century? Importantly, as it turns out, the spectral lines of a second star are never detected. This would require the one of the pair to be relatively faint. In addition, it was rather suspicious to 19th century astronomers that after theoretical calculations of the Cepheid's mass and radius (using visible magnitudes and colors) a clear trend in ρ versus Π emerges. This is of course the relation derived in Equation 2.43. These reasons and more led to the abandonment of the binary theory and acceptance of new single-star models.

Taking the models of the previous sections to be approximately true we are still left without a physical mechanism. This mechanism must satisfy dual requirements.

First, because Cepheids are a rare phenomena, the mechanism must not allow all stars to have self-reinforcing pulsation. Second, the mechanism must provide energy to an appropriate depth. The first requirement requires that a non-Cepheid that has been disturbed, possibly by an approaching star, has damped rather than driven oscillations. The second requirement is actually very useful in the fact that it eliminates any nuclear process. Eddington originally proposed the nuclear mechanism as a type of heat-valve when using the analogy of a Cepheid as a heat engine. It seems reasonable that nuclear processes which generate energy are related to both the temperature and density of the gas. When the gas is compressed, increases in temperature and density should spur more nuclear reactions and the star expands. Again, though, this process applies to all stars. In addition, our second requirement is violated: the greatest effect would be seen at the center of the star where density and temperature are large, but pulsation has been shown to only occur in the outer layers.

Eddington later went on to propose a different kind of heat engine wherein the 'valve' is varying instead of the amount of heat. He suggested, correctly, that this was due to a change in the absorption law for opacity within the star. Typically, for stellar material it is assumed that the opacity varies according to

$$\kappa \propto \frac{\rho}{T^{\frac{7}{2}}}. \tag{2.48}$$

However, Eddington suggested that under some unknown hypothetical conditions the exponent may be changed to become

$$\kappa \propto \frac{\rho}{T^{\frac{5}{2}}}. \tag{2.49}$$

This slight change in exponent has the effect of making the star more 'heat-tight'

when compressed than when it is expanded. The 'leakiness' of Eddington's valve is dependent on the proportionality between ρ and T. Because under normal circumstances the temperature goes like $T^{-3.5}$, the opacity of compressed layers tends to increase rather then decrease. Changing the exponent to $T^{-2.5}$ drastically changes the situation, and opacity increases during compression (Eddington, A. S. 1926).

Only later (Zhevakin 1963) was it found by that this valve is actually the absorption of partial-ionization layers in a star, typically helium, which increase absorption during times of compression. Thus work is done on the gas (by ionizing Helium) instead of raising the temperature of the layer. This high-opacity layer is pushed outward by radiation pressure until the density and temperature is low enough to allow recombination of the ionized Helium; the layer collapses inward and the process begins again.

CHAPTER III

DATA ANALYSIS AND METHOD

The data used in this thesis was collected over a period of three years at Fred Whipple Observatory 1.2-meter telescope in southern Arizona. Observations were made through three wide-band filters: B, V, and I, with central wavelengths near 440, 555, and 830 nanometers, respectively. The galaxy we are interested in, M33, is centered at (RA, Dec) $= 1h\ 33m\ 50.9s, +30^o\ 39'\ 36''$ (J2000). M33 was broken up into several observing regions; the field used in this thesis was labeled "C" and "Y3", depending on the camera being used to obtain the images. The approximate center and extent of the field is shown by the white box in Figure 1. The images had been previously reduced, but had never been analyzed as a complete three-year data set.

PSF photometry was carried out using the DAOPHOT/ALLSTAR and ALLFRAME packages developed by Dr. Peter Stetson. We analyzed 265, 78 and 35 frames in the V, I and B filters, respectively. Over 40,000 stellar objects were detected. We then matched our images to a world-coordinate system and corrected our magnitudes to the standard system, which involved zeropoint and color corrections. Finally, a variable search was performed, utilizing both the TRIAL software package developed by Dr. Peter Stetson and additional software developed at A&M by Dr. Anne Pellerin

Photometry

The data was initially processed using the DAOPHOT/ALLSTAR package (Stetson 1987), which carries out photometry in each of our images. Photometry is a technique used to measure the flux of a point source by counting the electrons collected in a CCD

detector. These electrons, originally created by photons incident on the detector, are linearly correlated to the apparent brightness of a star. Since our fields contain stars that are very close to each other, the proper method for performing this photometry is to derive a Point Spread Function (PSF) using bright isolated stars in each image and then scale this function to fit all fainter objects. PSF stars may vary from image to image.

Once photometry of each individual frame has been completed we use the (x,y) coordinates of each star determined through PSF fitting to correlate stars from one image to the next. This is done using two programs called DAOMATCH and DAOMASTER. We then used these coordinate transformations to make a median image of the field with a program called MONTAGE. This median image is then run through PSF photometry again several times, using a process of image subtraction with ALLSTAR, then finding additional stars and adding these new stars to the list. This process found 3.2×10^4, 4.0×10^4, and 2.7×10^4 objects in V, I, and B, respectively.

The process of inter-frame magnitude correlation is done by using ALLFRAME. This process measures the magnitude of every star in the list for each individual frame and filter. This generated approximately 10^7 photometric measurements. We then would like to know how magnitudes scale from frame to frame. To do this we chose reference stars based on their magnitude, error, and whether or not they appeared in all frames. A magnitude versus error plot is shown in Figure 6.

We then set the frame-to-frame zeropoint magnitude based on these "secondary standard stars" using a program called CCDAVE. Knowing the relative magnitude from frame-to-frame and the date of each magnitude allows us to make lightcurves such as
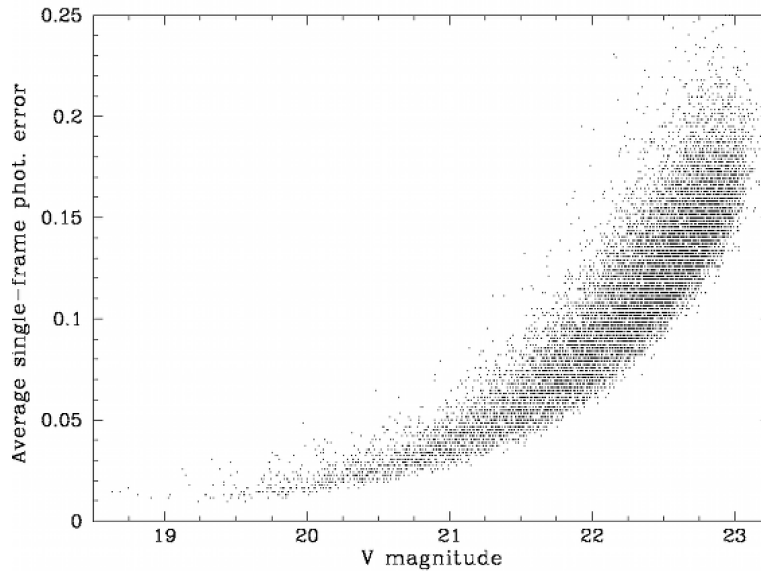
FIG. 6.— Photometric error as a function of magnitude, indicating typical photometry.

the ones shown in Figure 7 which illustrate magnitude variation from one observation to the next.

Photometric calibration

The instrumental magnitudes for all stars must now be transformed to the standard system. This is usually done by observing so-called "standard stars" at a variety of elevations during several clear nights within the observing season. However, the DIRECT project had to cover a lot of fields in M31 and M33 each night and thus had very little time to devote to this type of observations.

M31 and M33, along with many other Local Group galaxies, were recently surveyed by a collaboration led by Dr. Phil Massey of the United States Naval Observatory in Flagstaff, AZ. The scientific goal of their project was to identify very massive stars in these galaxies through accurately-calibrated broad- and narrow-band photome-
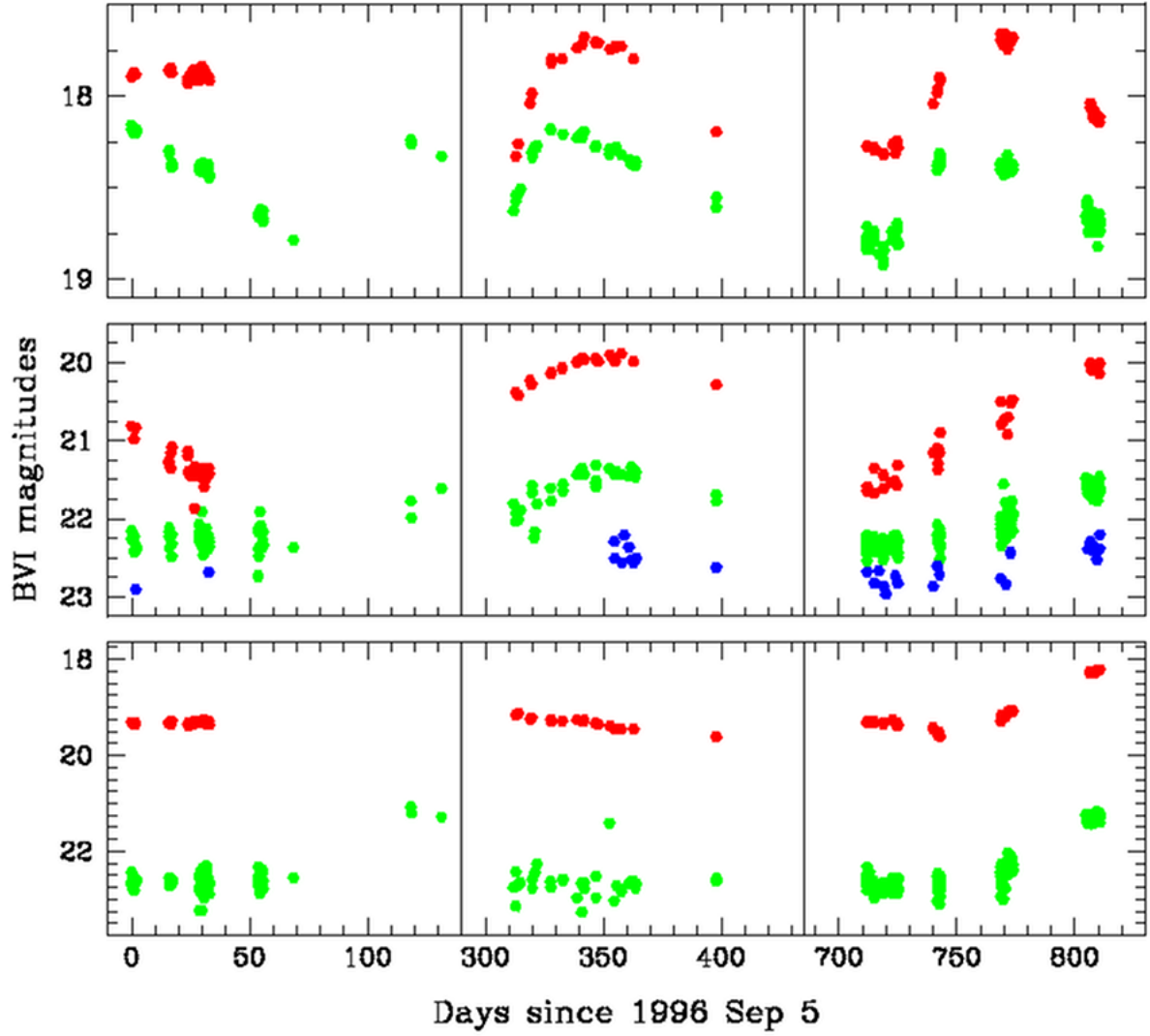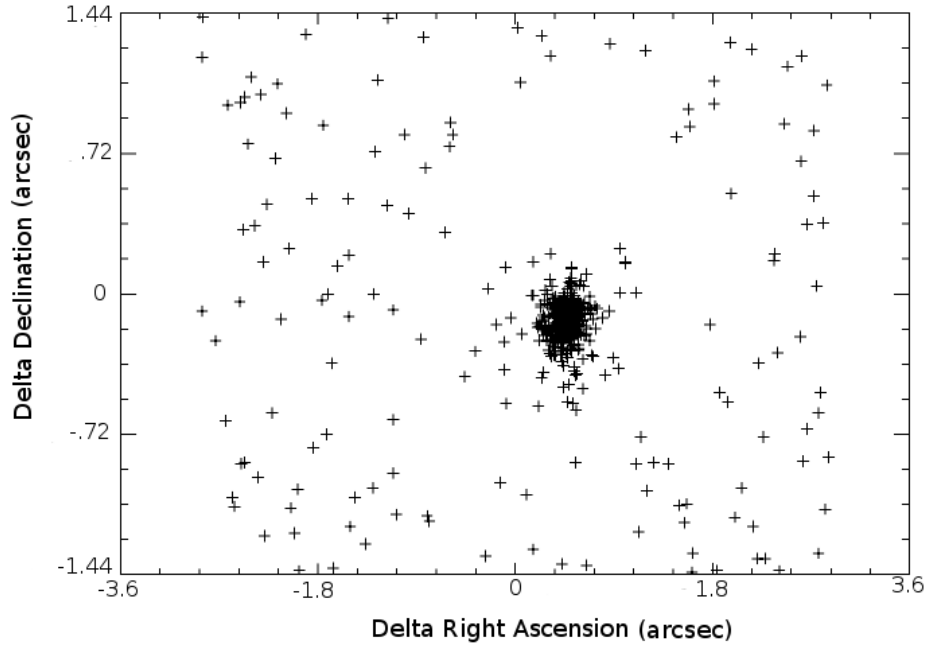
FIG. 7.— Three sample lightcurves.

FIG. 8.— RA-Dec coordinate matching, showing a match within .3".

try. These observations were presented in Massey et al. (2006). While accurately calibrated, this survey has no variability information.

Given the relative paucity of standard star observations in the DIRECT project, we decided to calibrate our photometry by matching bright stars in our field to the Massey et al. database. However, to do this we first needed to map the CCD x-y coordinates to celestial coordinates (also known as a World Coordinate System transformation). To set the world coordinate system of our images, we used the IMWCS program which is part of the WCSTools package (Mink 2002). Once we have the Right Ascension (RA) and Declination (Dec) of our stars we can match them to the database of Massey et al. Figure 8 indicates the results of this match, including a tight, well-matched set of stars near position (0,0).

These matched stars are then used to find the transformation from instrumental to standard magnitudes. This process involves two steps. First, we must correct for the slight differences in central wavelength and bandwidth of the filters originally used to define the standard system and those used in the cameras at the Whipple Observatory. Additionally, this correction takes care of the different relative efficiencies of the photoelectric equipment used to originally define the standard system and modern CCD cameras. This process is known as "color-term correction." Hicken et al. (2009) determined very accurate color terms for the cameras we used, so we adopt their equations listed below:

$$(v_{obs} - V_{std}) \quad = \quad color\ term \times (B - V)_{std} \tag{3.1}$$

$$= \quad 0.0366 \times (B - V)_{std} \tag{3.2}$$

$$(b - v)_{obs} \quad = \quad 0.8928 \times (B - V)_{std} \tag{3.3}$$

$$(v - i)_{obs} \quad = \quad 1.0166 \times (V - I)_{std}. \tag{3.4}$$

These equations can be seen graphically in Figure 9, which shows that by using the color terms we are essentially making our colors equivalent to those in the standard catalog. The left panels of Figure 9 show the uncorrected relation between instrumental and standard magnitudes, while the right panels show the same relations after we applied the color-term corrections of Hicken et al. The y-axis intercept defines the other term in this calibration process, which is known as the "zeropoint" value. We derived zeropoints of $V = 2.904$, $I = 2.731$, and $B = 2.291$ magnitudes.
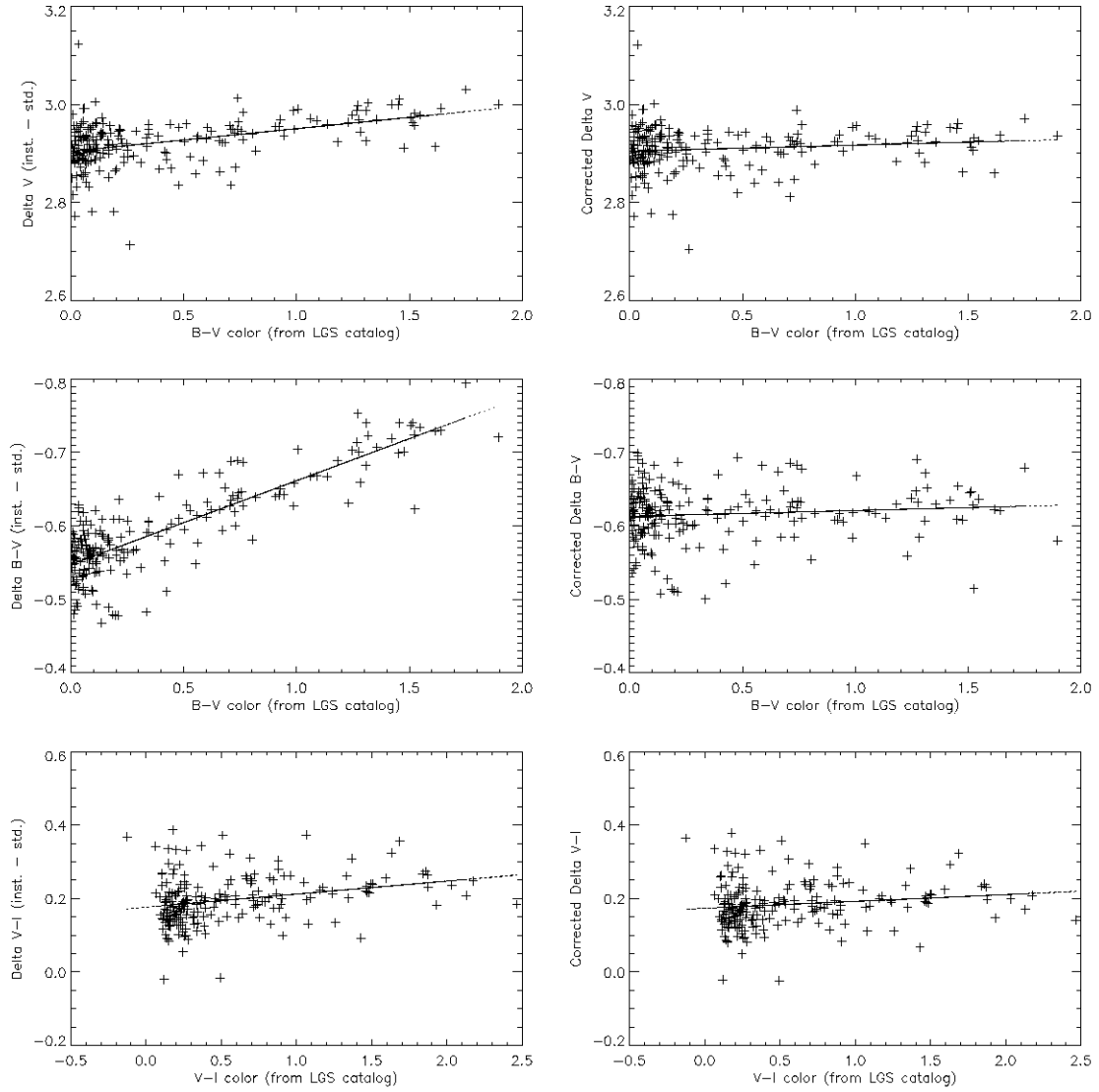
FIG. 9.— Determination of photometric zeropoints using colorterms from Hicken et al. (2009).

Thus, the equations we used to correct our magnitudes are the following:

$$V_{apparent} = v_{obs} - V_{zpt} - color\ term_{(v-V)} \times \frac{(b_{obs} - B_{zpt}) - (v_{obs} - V_{zpt})}{color\ term_{(B-V)}} \quad (3.5)$$

$$B_{apparent} = V_{apparent} + \frac{(b_{obs} - B_{zpt}) - (v_{obs} - V_{zpt})}{color\ term_{(B-V)}} \quad (3.6)$$

$$I_{apparent} = V_{apparent} - \frac{(v_{obs} - V_{zpt}) - (i_{obs} - I_{zpt})}{color\ term_{(V-I)}}. \quad (3.7)$$

Variable search

Once the magnitude of each star in every frame is known, it becomes possible to look for variations as a function of time, such as the ones shown in Figure 7. Our variable search was performed using the modified Welch-Stetson variability index (Stetson 1996), which identified over 1,200 objects as possible variables. A plot of variability index versus magnitude is shown in Figure 10. As part of this variability search, a program called TRIAL will output a data file for each suspected variable containing the time of each observation and the calibrated magnitude of that star in that particular image. These so-called "light curve" files are then run through a template-fitting algorithm developed by Dr. Peter Stetson and implemented at A&M by Dr. Anne Pellerin. These template Cepheid curves are similar to the one shown in Figure 3. By stretching and phasing a template curve, candidate variables can then be identified as Cepheids. This process eventually found approximately 100 Cepheids of varying periods. In addition, the algorithm fits both a constant and a linear equation to the light curve. Light curves which were better represented by constants were thrown out, and those that are better represented by a constant (rather than a model Cepheid light-curve) were flagged as possible long-period variables. Histograms of the resulting χ^2 values are shown in Figure 11. After the fitting was performed, a variable must have a $\chi^2 < 60$ in order to be considered a candidate Cepheid.
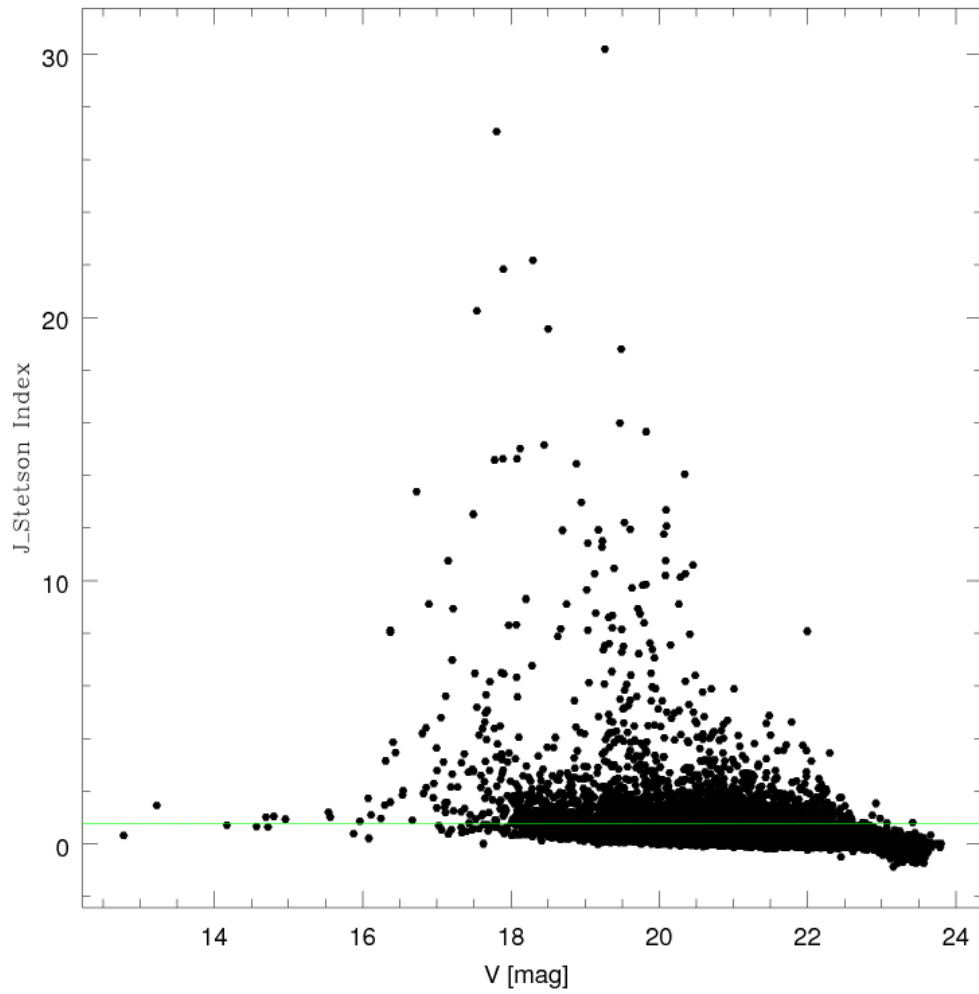
FIG. 10.— A graph of the Stetson variability index for all stars, showing the cutoff at $J_S = .75$.
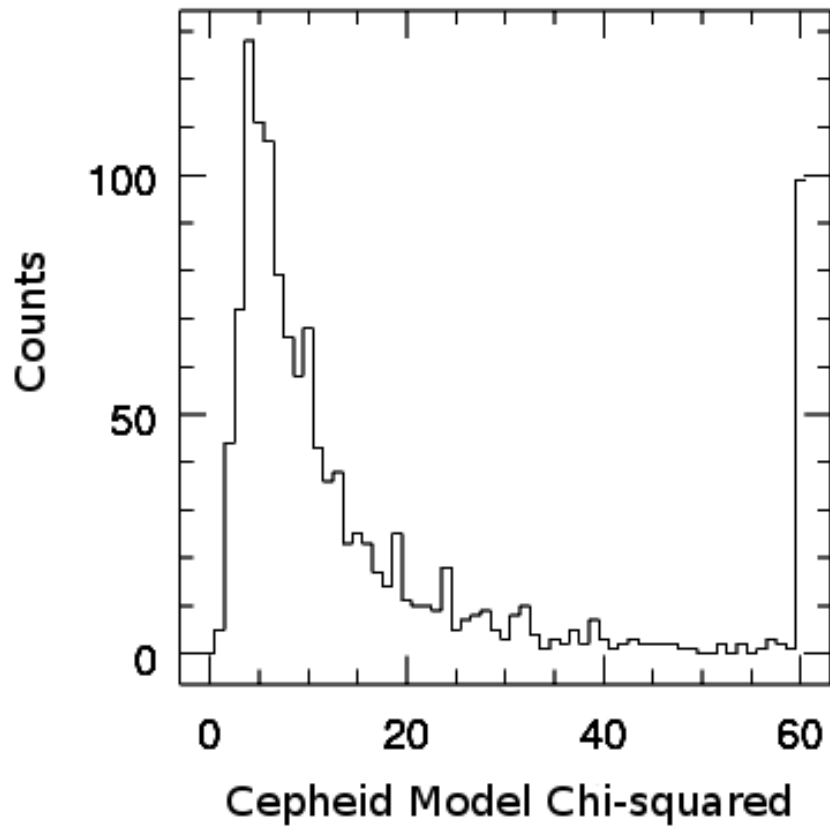
FIG. 11.— A histogram of the Cepheid fitting chi-squared values.

CHAPTER IV

CONCLUSIONS AND DISTANCE TO M33

After completing the variable search and classification we have a full set of possible Cepheid variable stars which can be used to estimate the distance to M33. To get a precise and accurate distance, several additional cuts and corrections to the sample must be made. For instance, the flux of some of our candidate Cepheids will be contaminated by light from nearby, unresolved stars and these objects must be removed from the sample. Other objects will not be subject to this contamination but will lie along a line of sight that contains a larger amount of interstellar dust, an effect that must be corrected.

Cepheid selection criteria

With our full list of possible variables, approximately 10^3 objects, we first apply a simple χ^2 cut to throw out variables which had poor model lightcurves fit to the data. An appropriate value of χ^2 was chosen by considering Figure 11 shown in the previous chapter. Immediately following the cut in model χ^2 we require that the amplitude ratio of the candidate be in within a certain range. We chose to cut using the ratio of the amplitudes in the I and V band, as shown in Figure 12. This ratio arises from the blackbody nature of the Cepheid spectral energy distribution. As the Cepheid changes in temperature, the flux emitted in the V band will fluctuate more than the flux emitted in the I band. The expected trend is such that the ratio of I-to-V amplitude should be about 0.4. We adopted a very generous range of amplitude ratios that spanned 0.2 to 0.65, depicted in Figure 12.
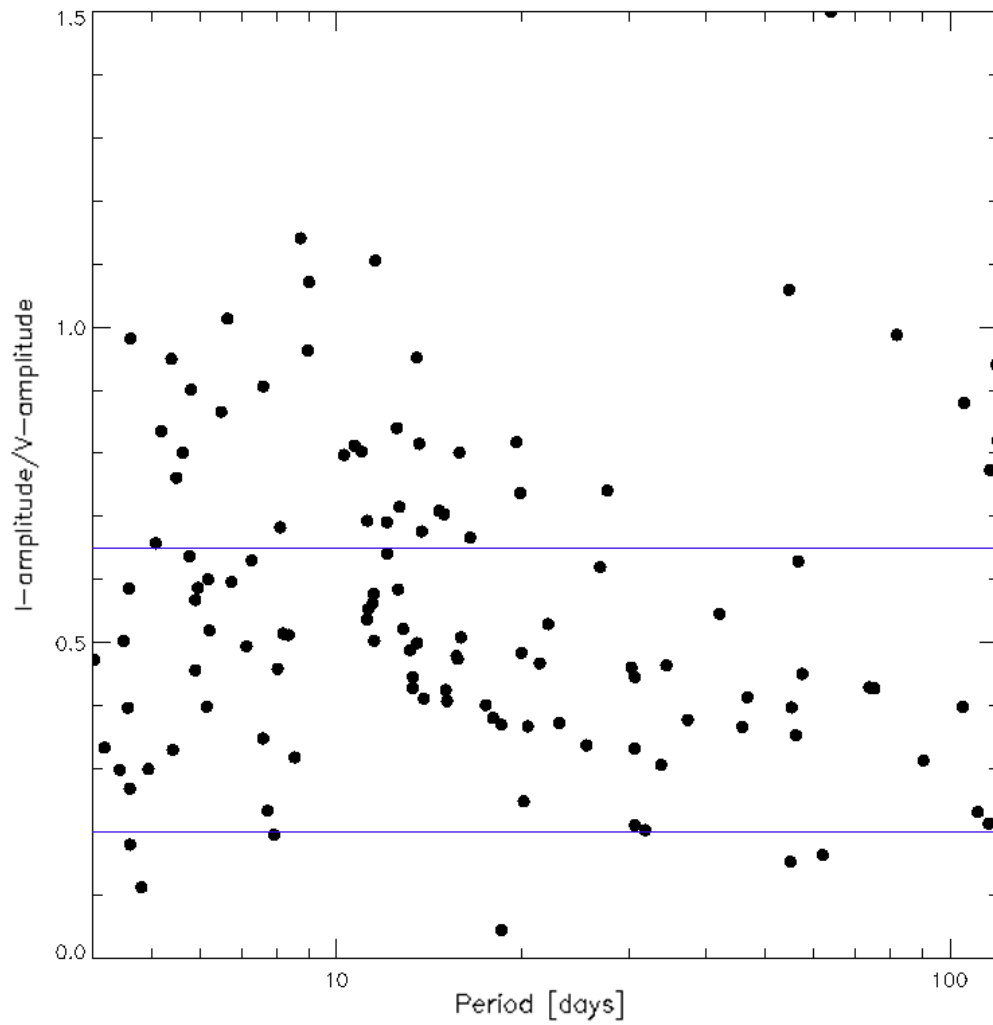
FIG. 12.— A graph of all candidate Cepheids with our cut in I-to-V amplitude ratio indicated by the blue lines.

After cutting by χ^2 and by the amplitude ratio criterion we had reduced our number of possible variables to approximately 100 objects. These final objects were then checked using their deviation from the fiducial Period-Luminosity (P-L) relation using a procedure developed by Dr. Barry Madore. This test is shown in Figure 13. Plotted in the top section is the difference between measured magnitude and the best fit P-L relation magnitude (for both V and I on the X and Y axes, respectively). The trend which becomes visible when these two variables are plotted against each other represents another well known property of Cepheids. Due to the intrinsic width of the instability strip, some Cepheids are intrinsically bluer (or redder) than others. This trend from blue to red can be seen as the diagonally-rising line in the top panel of Figure 13. At the tip of this line a few more candidate Cepheids can be seen. These are identified as highly reddened Cepheids, most likely due to dust. This diagonally-rising direction is the only direction in which an object can be reddened by dust. Therefore we make our cut using the P-L relation by eliminating those candidates which are not near this blue-red line or near the red tip. The objects which pass the cut are shown in red boxes in Figure 13, where the P-L relation has also been plotted to show the effect of this cut on our I-band. Approximately half of our candidates were rejected using this method.

P-L relations and reddening

Having now made several cuts, we have reduced our possible Cepheid pool from approximately 1000 to around 50. These final candidates are the most reliable sample for performing distance measurements. A few of their lightcurves are shown in Figure 14. Their location on the color-magnitude diagram is shown in Figure 15.
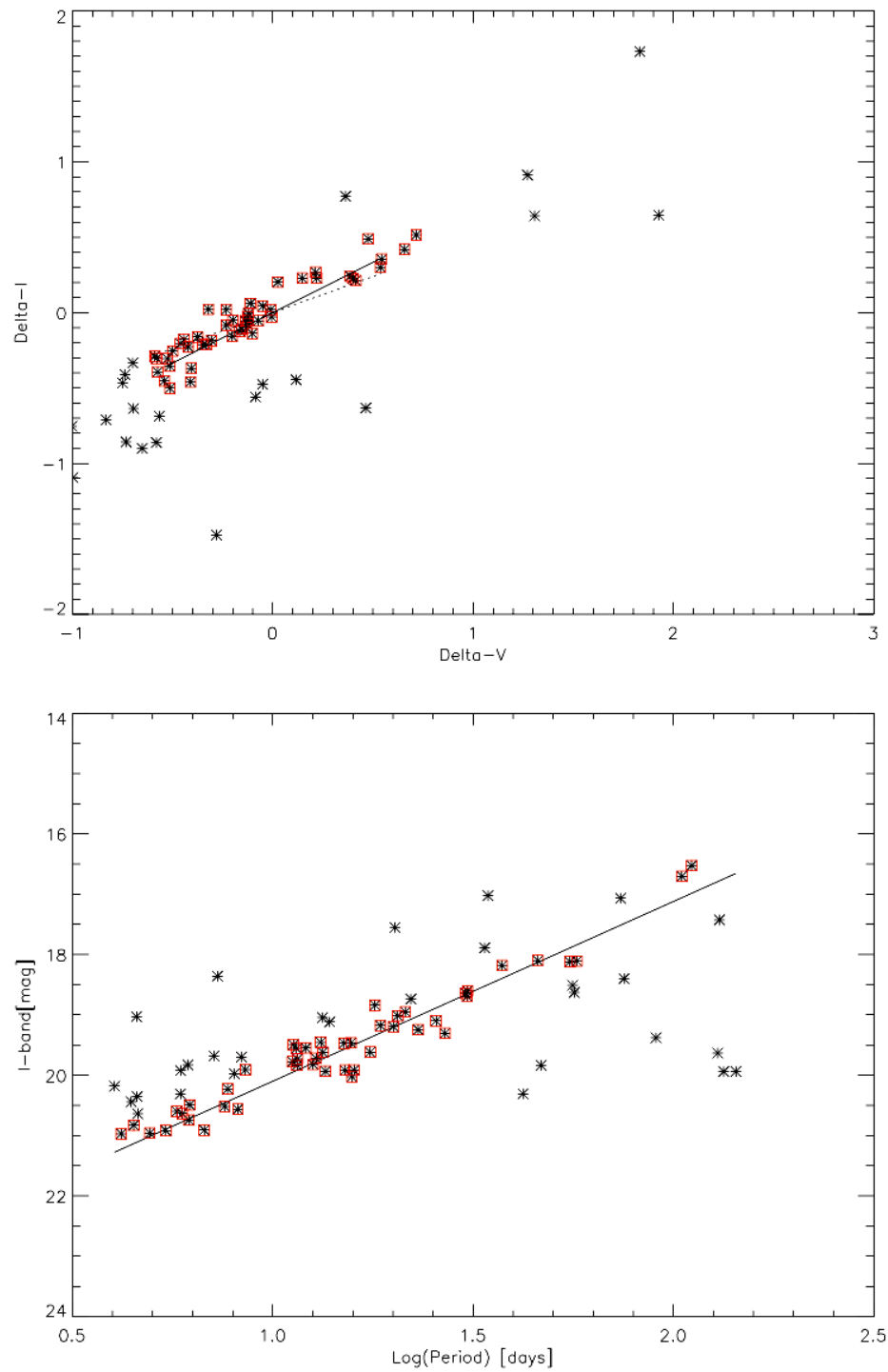
FIG. 13.— The P-L relation cut, where red boxed objects were kept and unboxed were thrown out.
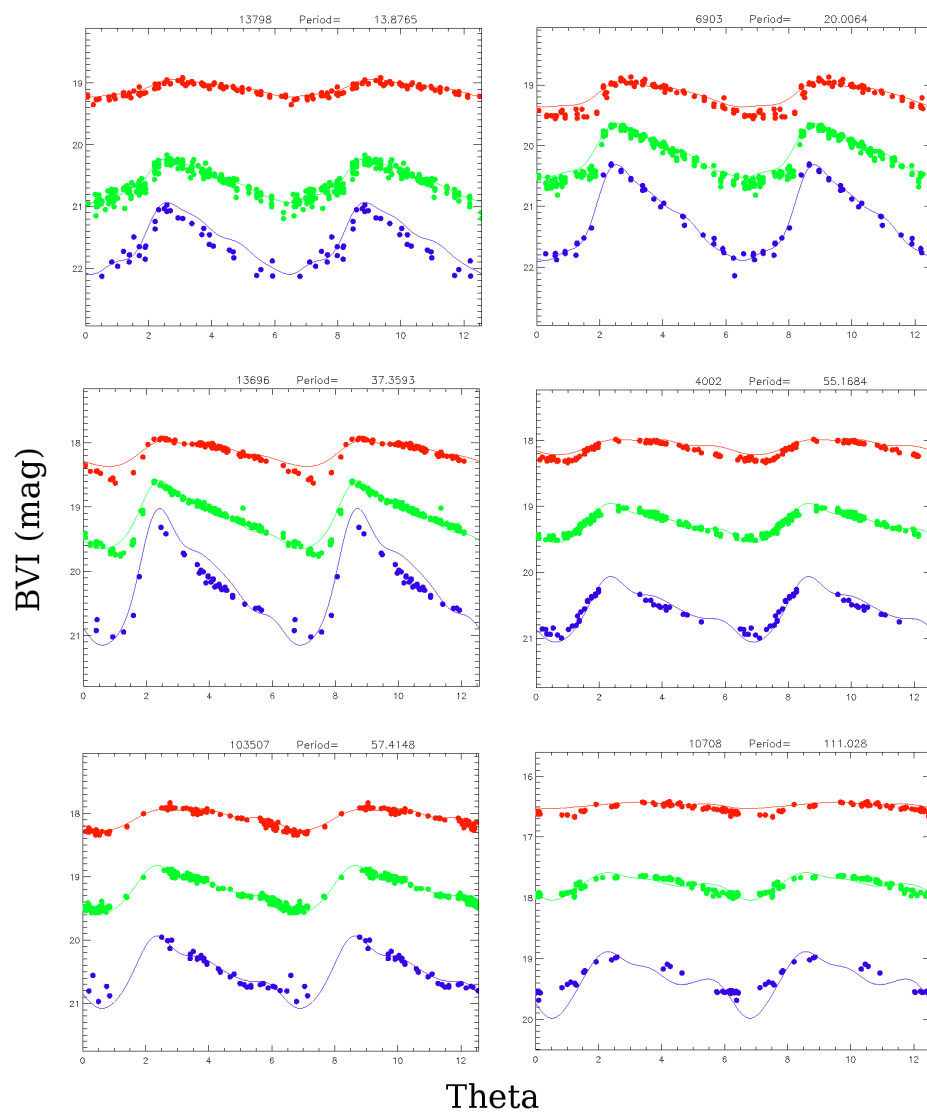
FIG. 14.— A sample of some well-defined Cepheid light curves from our data.
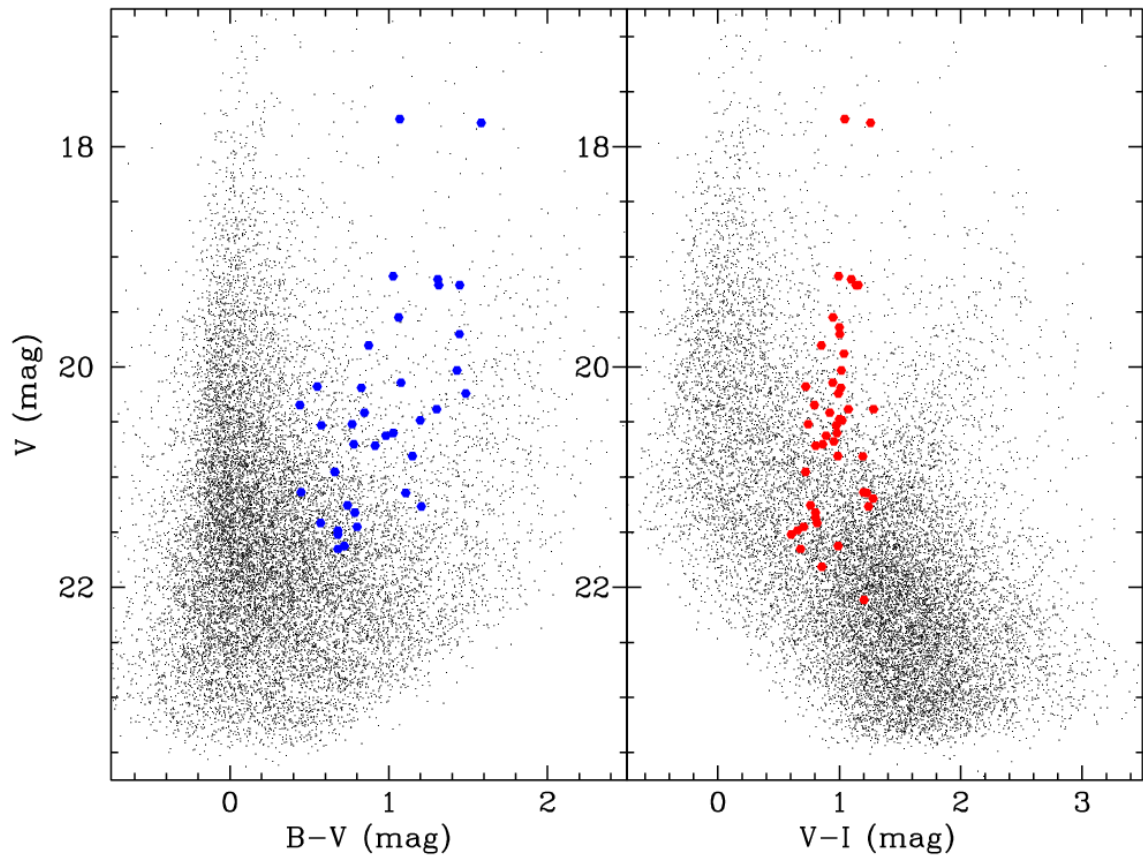
FIG. 15.— Color-magnitude diagram showing the distribution of stars and Cepheids (shown in color).

In order to derive a distance to M33 using these Cepheids, we first need to adopt a fiducial set of Period-Luminosity relations. These come from the OGLE II project which discovered over 600 Cepheids in the Large Magellanic Cloud (LMC) (Pietrzynski & Udalski 1999). The Cepheids which compose the data set have periods between 2 and 30 days, and were observed in the B, V, and I filters, making them ideal for our data. The fiducial P-L relations take the form:

$$m_B = -2.439 (\log P - 1) + 14.929, \sigma = 0.239 \tag{4.1}$$

$$m_V = -2.779 (\log P - 1) + 14.287, \sigma = 0.160 \tag{4.2}$$

$$m_I = -2.979 (\log P - 1) + 13.615, \sigma = 0.107 . \tag{4.3}$$

However, the magnitudes in these equations are apparent magnitudes, owing to the distance to the LMC. In order to find the distance modulus μ to M33 then we must take into account the distance to the LMC; a number which is somewhat controversial. In this thesis we adopt an LMC distance of 48.3 $\pm$1.4 kpc, corresponding to a distance modulus of $\mu_{LMC} = 18.42 \pm .03$ mag (Fitzpatrick et al. 2003). Subtracting this number from Equations 4.1, 4.2, and 4.3 to get the absolute magnitude M_B, M_V, and M_I. Then we form the distance moduli in each observed band (b, v, and i) using $\mu = m - M$:

$$\mu_B = b - [-2.439 (\log P - 1) - 3.491] \tag{4.4}$$

$$\mu_V = v - [-2.779 (\log P - 1) - 4.133] \tag{4.5}$$

$$\mu_I = i - [-2.979 (\log P - 1) - 4.805]. \tag{4.6}$$

Period-Luminosity relations for the final set of M33 Cepheids are plotted in Figure 16. We fix the slope of these relations to those of the LMC relations and solve for the distance modulus. This figure includes an additional panel which plots the Wesenheit
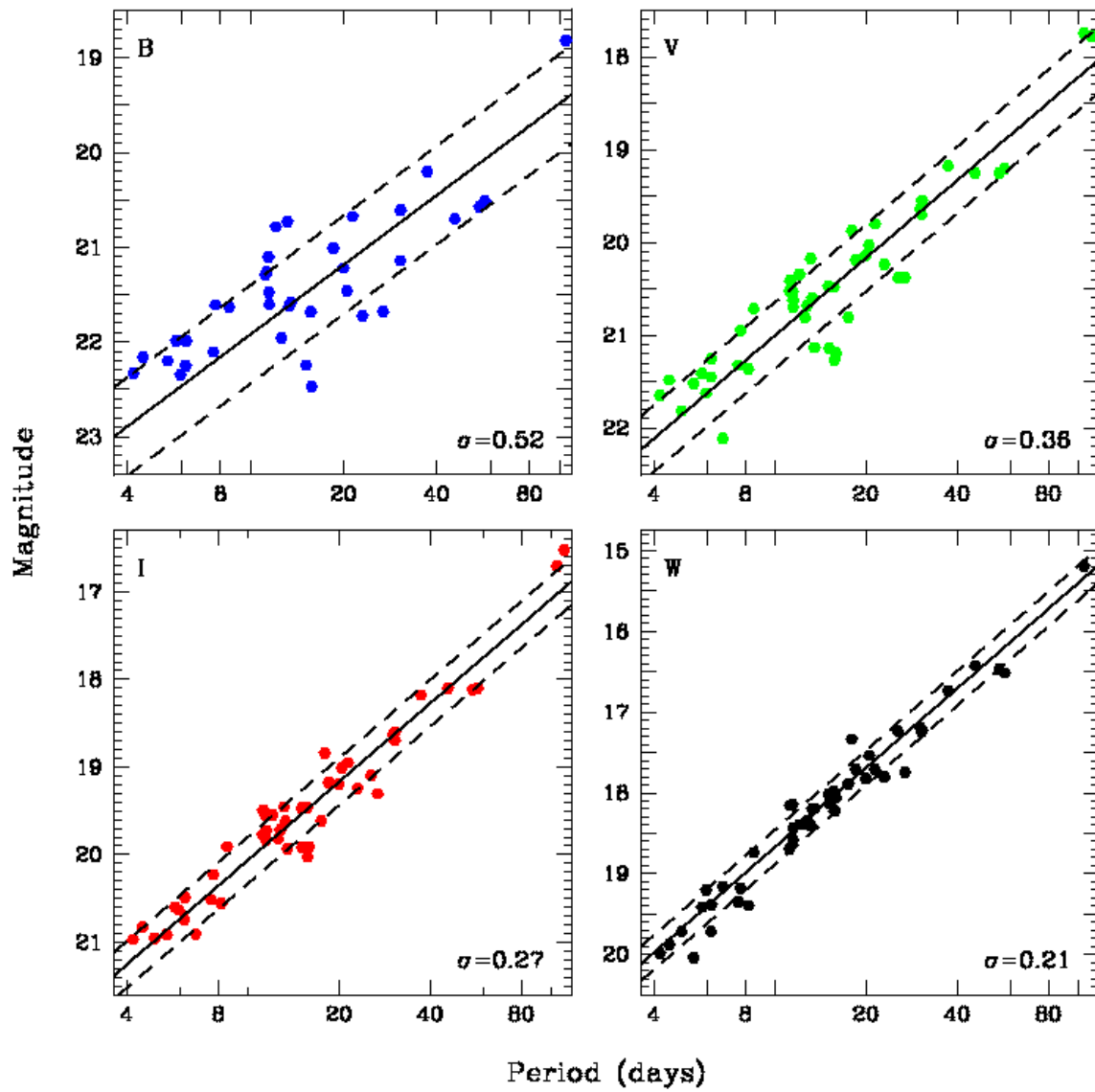
FIG. 16.— Period-luminosity relations for our final set of Cepheids.

relation $W = 2.45 \ (V - I)$ (to be described later). We find the following distance moduli: $\mu_B = 25.299$, $\mu_V = 25.103$, $\mu_I = 24.848$, and $\mu_W = 24.604$.

The range of μ values found above is due to the fact that there exists a certain amount of dust between the observer and Cepheid, so all objects will suffer from a reduction in the flux, a process called "extinction". This process preferentially affects shorter wavelengths, giving rise to increasingly larger apparent distance moduli as a function of inverse wavelength. All of this can be accounted for, however, using a model for the interstellar extinction of light (Cardelli et al. 1989). Assuming a value of total-to-selective extinction R_V $(= \frac{A_V}{E(B-V)})$ of 3.1 we can then use models that span the ultraviolet, optical and infrared regions of the electromagnetic spectrum to account for this effect. This is done by fitting curves to the observed magnitudes in several bands. An equivalent method is fitting it to the distance moduli in each band, which we do in Figure 17. The red line in Figure 17 consists of the infrared model, and the green line refers to the optical/UV model. By extending the infrared model all the way to $\lambda^{-1} = 0$, or $\lambda = \infty$, we are essentially modelling what the magnitude would be like without any dust effects. Thus the point at which the infrared model intersects the y-axis is our true distance modulus, μ_0. Using the μ values calculated in each band and then performing the extinction correction we arrive at a value of $\mu_0 = 24.49 \pm 0.01$ mag. However, this is not the only source of uncertainty in the distance estimate. Other sources of error are characterized in the next section.

Error budget and distance to M33

Several sources of uncertainty must be included in our analysis. The photometry was calibrated against the database of Massey et al. (2006) and exhibited an overall
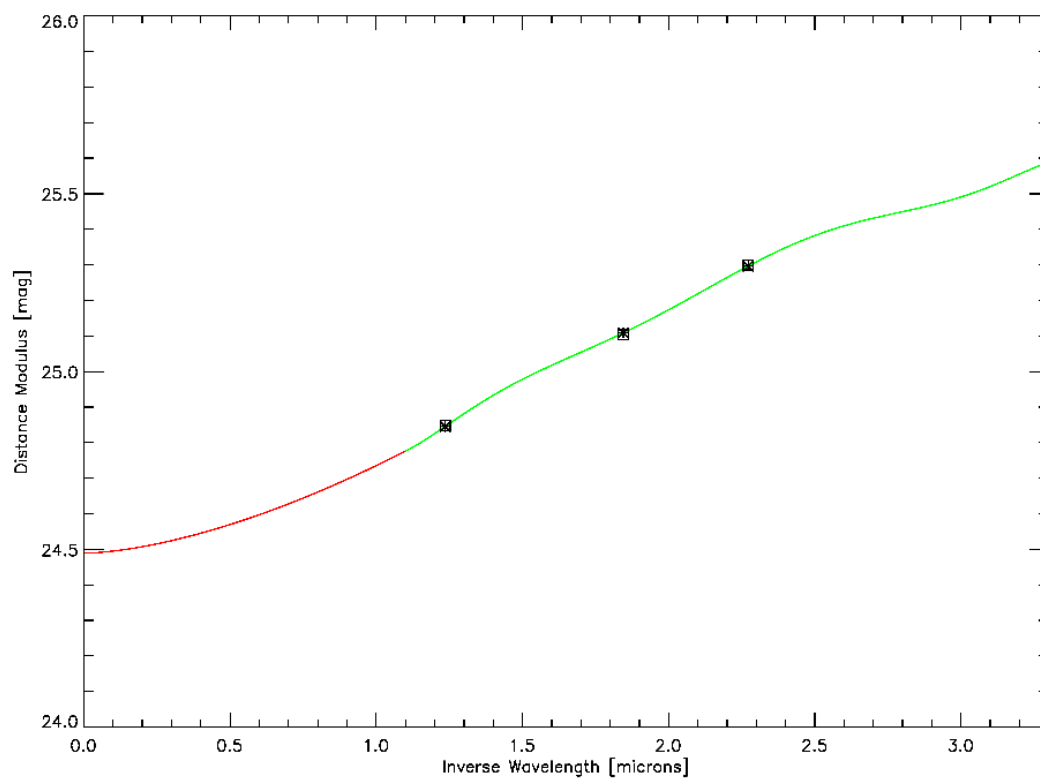
Fig. 17.— Distance determination using extinction correction.

uncertainty of $\pm$ 0.04 (statistical) and $\pm$ 0.03 mag (systematic). In addition, the uncertainty in the distance modulus of the LMC was estimated to be $\pm$ 0.03 mag. Thus our total error in the distance modulus is ± 0.07, or $\mu_0 = 24.49 \pm .07$ mag. This distance modulus corresponds to a distance of $D = 790 \pm 25$ kiloparsecs.

REFERENCES

Cardelli, J. A., Clayton, G. C., & Mathis, J. S. 1989, Astrophysical Journal, 345, 245

Eddington, A. S. 1926, The Internal Constitution of the Stars (Cambridge University Press), 181–202

Eddington, Sir, A. S. 1930, Monthly Notices of the Royal Astronomical Society, 91, 109

Fitzpatrick, E. L., Ribas, I., Guinan, E. F., Maloney, F. P., & Claret, A. 2003, Astrophysical Journal, 587, 685

Hicken, M., Challis, P., Jha, S., Kirshner, R. P., Matheson, T., Modjaz, M., Rest, A., & Wood-Vasey, W. M. 2009, ArXiv e-prints: arxiv.org/abs/0901.4787

Hubble, E. 1929, Proceedings of the National Academy of Science, 15, 168

Leavitt, H. S., & Pickering, E. C. 1912, Harvard College Observ. Circ., 173, 1

Massey, P., Olsen, K. A. G., Hodge, P. W., Strong, S. B., Jacoby, G. H., Schlingman, W., & Smith, R. C. 2006, Astronomical Journal, 131, 2478

Mink, D. J. 2002, in Astronomical Society of the Pacific Conference Series, Vol. 281, Astronomical Data Analysis Software and Systems XI, ed. D. A. Bohlender, D. Durand, & T. H. Handley, 169

Pietrzynski, G., & Udalski, A. 1999, Acta Astronomica, 49, 543

Stetson, P. B. 1987, Publications of the Astronomy Society of the Pacific, 99, 191

—. 1996, Publications of the Astronomy Society of the Pacific, 108, 851

Zhevakin, S. A. 1963, Annual Review of Astronomy and Astrophysics, 1, 367

CONTACT INFORMATION

Name: Andrew Kenneth Bradshaw

Professional Address: Department of Physics
Texas A&M University
4242 TAMU
College Station, TX 77843-4242

Email Address: andrew@andrewnomy.com

Education   B.S., Physics, Texas A&M University